2015

The Interferon-stimulated gene Ifi27l2a restricts West Nile virus infection and pathogenesis in a cell-type and region-specific manner

Tiffany M. Lucas
Washington University School of Medicine

Justin M. Richner
Washington University School of Medicine

Michael S. Diamond
Washington University School of Medicine

J. Virol. doi:10.1128/JVI.02463-15

The Interferon-stimulated gene Ifi27l2a restricts West Nile virus infection and pathogenesis in a cell-type and region-specific manner

Tiffany M. Lucas[1], Justin M. Richner[1], and Michael S. Diamond[1,2,3,4,]

Departments of Medicine[1], Pathology & Immunology[2], Molecular Microbiology[3], and the Center for Human Immunology and Immunotherapy Programs[4], Washington University School of Medicine, St Louis, MO 63110 USA.

Corresponding author: Michael S. Diamond, M.D., PhD, Departments of Medicine, Molecular Microbiology and Pathology & Immunology, Washington University School of Medicine, 660 South Euclid Avenue, Box 8051, St Louis. Missouri 63110. Tel: 314-362-2842, Fax: 314-362-9230, Email: diamond@borcim.wustl.edu

Running title: The ISG Ifi27l2a restricts WNV infection in the CNS

Figures 10: **Tables: 1**

ABSTRACT

The mammalian host responds to viral infections by inducing expression of hundreds of interferon-stimulated genes (ISGs). While the functional significance of many ISGs has yet to be determined, their cell-type and temporal nature of expression suggests unique activities against specific pathogens. Using a combination of ectopic expression and gene silencing approaches in cell culture, we previously identified *Ifi27l2a* as a candidate antiviral ISG within neuronal subsets of the central nervous system (CNS) that restricts West Nile virus (WNV) infection, an encephalitic flavivirus of global concern. To investigate the physiological relevance of Ifi27l2a in the context of viral infection, we generated *Ifi27l2a*$^{-/-}$ mice. Although adult mice lacking *Ifi27l2a* were more vulnerable to lethal WNV infection, viral burden was greater only within the CNS, particularly in the brain stem, cerebellum, and spinal cord. Within neurons of the cerebellum and brain stem, in the context of WNV infection, a deficiency of Ifi27l2a was associated with less cell death, which likely contributed to sustained viral replication and higher titers in these regions. Infection studies in primary cell culture revealed that *Ifi27l2a*$^{-/-}$ cerebellar granule cell neurons and macrophages but not cerebral cortical neurons, embryonic fibroblasts, or dendritic cells sustained higher WNV infection compared to wild-type cells, and this difference was greater under conditions of IFN-β pretreatment. Collectively, these findings suggest that Ifi27l2a has an antiviral phenotype in subsets of cells, and that at least some ISGs have specific inhibitory functions in restricted tissues.

43 **IMPORTANCE STATEMENT**

44 The interferon-stimulated gene, *Ifi27l2a*, is expressed differentially within the central
45 nervous system upon interferon stimulation or viral infection. Prior studies in cell culture
46 suggested an antiviral role for Ifi27l2a during infection by West Nile virus (WNV). To
47 characterize its antiviral activity *in vivo,* we generated mice with a targeted gene deletion of
48 *Ifi27l2a*. Based on extensive virological analyses, we determined that Ifi27l2a protects mice from
49 WNV-induced mortality by contributing to the control of infection of the hindbrain and spinal
50 cord, possibly by regulating cell death of neurons. This antiviral activity was validated in granule
51 cell neurons derived from the cerebellum and in macrophages but was not observed in other
52 cell types. Collectively, these data suggest Ifi27l2a contributes to innate immune restriction of
53 WNV in a cell-type and tissue-specific manner.
54

INTRODUCTION

West Nile virus (WNV) is a positive-stranded, enveloped RNA virus that belongs to the Flavivirus genus of the *Flaviviridae* family. WNV and related flaviviruses typically are transmitted by arthropod vectors and include members that cause encephalitis (e.g., Japanese encephalitis virus (JEV), Saint Louis encephalitis virus (SLEV), and tick-borne encephalitis virus (TBEV)) or systemic and/or visceral disease (e.g., Dengue virus (DENV) and yellow fever virus (YFV)). WNV transmission occurs between *Culex* species mosquitoes and selected avian hosts, with incidental, dead-end infection of horses, humans, and other vertebrate animals. Humans can develop severe disease following WNV infection, as the virus can invade the central nervous system (CNS) and cause flaccid paralysis, meningitis, or encephalitis, often leading to long-term neurological sequelae or death (1). In the CNS, WNV replicates principally in neurons, and infection may lead to focal lesions, cell injury, and cell death within the brain and spinal cord (2-4). Factors governing WNV entry into and replication within the CNS are complex, and include age of the host, genetic background (5-8), quality of the immune response, and integrity of the blood-brain barrier (for review, 9, 10-12).

In response to viral infections, most mammalian cells secrete type I interferon (IFN), which promotes an antiviral state in an autocrine and paracrine manner by inducing expression of hundreds of interferon-stimulated genes (ISGs). The gene signature and inhibitory activity promoted by type I IFNs vary depending on the cell type, specific viral pathogen, and possible pathogen-induced immune evasion mechanisms. Within the CNS, the innate immune response must balance the need to restrict virus infection while simultaneously protecting non-renewable neurons. Indeed, selected regions of the brain and CNS have evolved distinct antiviral programs and mechanisms to restrict infection of different RNA and DNA viruses (13-18). Neurons derived from the cerebral cortex are more permissive to infection by multiple viruses, with IFN-β pretreatment only minimally reducing infection of several viruses (14). In comparison, granule cell neurons (GCN) derived from the cerebellum are less permissive to viral infection at baseline

state and produce a stronger antiviral response following IFN-β pretreatment. Microarray analysis revealed differences in the basal and induced expression of ISGs in GCN compared to cortical neurons (CN) (14). As an example, *Ifi27l2a* is an ISG expressed at higher levels in GCN compared to CN under basal conditions, after IFN-β pretreatment, or following WNV infection. Ectopic expression of *Ifi27l2a* in CN suppressed infection of a neurotropic flavivirus (WNV) and coronavirus (murine hepatitis virus (MHV)) but not an alphavirus (Venezuelan equine encephalitis virus (VEEV)). Reciprocally, gene silencing of *Ifi27l2a* in GCN resulted in enhanced WNV infection (14).

Ifi27l2a (also termed ISG12b) is a 7.9 kDa protein belonging to a larger family of genes that include related *Ifi27/IFI27* genes, and the human *IFI6-16* gene (19), which are distinguished by an "ISG12" motif of unknown function (20). Family members are small, highly hydrophobic and may be localized to either mitochondrial (21, 22) or nuclear membranes (23, 24), although the exact localization has not been fully elucidated. Several *Ifi27* genes are IFN-inducible (19) yet others are not, and among the family members, some orthologs are not conserved across species. As an example, *IFI6-16* is an *IFI27* human gene family member that inhibits infection of YFV, WNV, and hepatitis C virus (HCV) (25-28), but does not have an apparent ortholog in mice. Although *Ifi27l2a* is induced broadly in peripheral organs after IFN stimulation, in the brain it is expressed in selected regions during development in an age-dependent manner (29) with high levels within the hippocampus (30). Cell culture studies have suggested that some Ifi27 gene orthologs (e.g., ISG12a) promote apoptosis and cell death (21, 31, 32).

Ifi27l2a and its closest orthologs have been evaluated as candidate antiviral genes. Despite the strong upregulation of *Ifi27l2a* mRNA in lung tissues, largely by infiltrating immune cells, *Ifi27l2a*$^{-/-}$ mice were not more susceptible to influenza A virus (IAV) infection than wild-type (WT) mice (33). In contrast, ectopic expression of human *IFI27* inhibited HCV and Newcastle disease virus (NDV) infection in hepatocellular carcinoma cells; reciprocally, gene silencing of IFI27 resulted in increased HCV and NDV infection (28, 34). Apart from its possible antiviral

activity, Ifi27 genes may regulate inflammation, as mice lacking *Ifi27l2a* sustained less vascular injury (24) and exhibited less septic shock after administration of endotoxin (35).

To characterize further the antiviral effects of Ifi27l2a, we generated *Ifi27l2a*$^{-/-}$ mice directly in a C57BL/6 background. *Ifi27l2a*$^{-/-}$ GCN from the cerebellum and bone marrow-derived macrophages (Mϕ) supported higher levels of WNV infection. Following infection with WNV *in vivo*, *Ifi27l2a*$^{-/-}$ mice exhibited increased mortality and higher viral burden in the cerebellum, brain stem, and spinal cord. The enhanced viral burden in the cerebellum and brain stem of *Ifi27l2a*$^{-/-}$ mice was associated with less death of neurons at early stages of CNS infection. Our findings suggest that Ifi27l2a contributes to an antiviral state against WNV within the CNS, and protects subsets of cell types and regions of the brain against infection.

MATERIALS AND METHODS

Virus. A WNV-New York (WNV-NY) stock was generated in C6/36 *Aedes albopictus* cells (ATCC) from a single passage of strain 3000.0259 isolated from a mosquito in New York in 2000 (36). The WNV Madagascar strain (WNV-MAD) stock was generated by passaging virus in Vero or C6/36 cells as described previously (37). WNV titers were assessed by plaque assay on BHK21-15 cells (38, 39). All virus stocks were stored at -80°C.

Mice. WT C57BL/6 mice were obtained from Jackson Laboratory (Bar Harbor, ME). *Ifi27l2a*$^{-/-}$ (*ISG12b*; 76933) mice were generated at Washington University after receiving heterozygous sperm from C57BL/6 containing a deleted gene (*Ifi27l2a*$^{tm1(KOMP)Vlcg}$) from the Knockout Mouse Project Repository (KOMP, University of California, Davis). Sperm was used for *in vitro* fertilization of eggs from C57BL/6 recipient female mice. Heterozygous *Ifi27l2a*$^{+/-}$ mice were backcrossed to establish the *Ifi27l2a*$^{-/-}$ colony. *Ifi27l2a*$^{-/-}$ mice produced normal litter sizes of expected Mendelian ratios, with all progeny appearing healthy. All animals were maintained in the pathogen-free animal facility of Washington University School of Medicine.

Mouse infection experiments. The experimental protocols were approved by the Institutional Animal Care and Use Committee at the Washington University School of Medicine (Assurance Number: A3381-01). Studies were performed on sex- and age-matched mice between 11 and 12 weeks of age, Peripheral infection was performed by subcutaneous inoculation into the footpad with 10^2 PFU of virus diluted in 50 µl Hank's Balance Salt Solution (HBSS) with 1% heat-inactivated fetal bovine serum (HI-FBS). Survival analysis was followed for 30 days. For viral burden studies after subcutaneous infection, mice were sacrificed at days 2, 4, 6, 8, 10, and 14 and peripheral organ and CNS tissues were collected following extensive perfusion with PBS, and stored at -80˚C. Serum was collected after cardiac puncture according to standard procedures. Intracranial infection was performed by injecting 10^1 PFU of WNV-NY or WNV-MAD in 10 µl HBSS supplemented with 1% HI-FBS. For analysis of viral burden after

intracranial infection, brain and spinal cord tissues were collected at 3 and 5 days and processed as described for tissues from peripheral infection. Brains were divided by dissection into brain stem, cerebellum, olfactory bulb, grey matter (cerebral cortex) and subcortex (corpus callosum, hippocampus, thalamus, and hypothalamus). Plaque assays were performed as previously described with Vero cells (38). Levels of WNV RNA in serum were measured by quantitative reverse transcription-PCR (qRT-PCR) as described (38, 40).

Generation and infection of primary cell cultures. All primary cell culture preparation and virus infection studies were performed as described below. In some experiments, cells were pretreated with indicated doses of mouse IFN-β prior to infection.

***(a) Murine embryonic fibroblasts*.** Murine embryonic fibroblasts **(**MEFs) were generated from embryonic day 14 WT and *Ifi27l2a*$^{-/-}$ mice. Embryos were decapitated, livers were removed and remaining minced tissue was digested in 0.25% (w/v) trypsin for 10 min at 37˚C with periodic, gentle agitation and mechanical disassociation. Following trypsin neutralization with FBS, cells were cultured in DMEM supplemented with 20% HI-FBS, 1% HEPES, 1% Glutamax (Life Technologies), 100 U/ml penicillin and streptomycin (Gibco) and 1% non-essential amino acids (Gibco). Cells were infected at a multiplicity of infection (MOI) of 0.01. A subset of cells was pretreated with 5 U/ml of mouse IFN-β (*E. coli*-derived, PBL Assay Science) for 12 h prior to infection with WNV.

***(b) Macrophages and dendritic cells*.** Mϕ and dendritic cells (DCs) were generated as previously described (41) from bone marrow of WT or *Ifi27l2a*$^{-/-}$ mice. Mϕ and DCs were stimulated in culture for 8 days with either 40 ng/ml recombinant murine M-CSF (Peprotech) or 20 ng/ml recombinant murine IL-4 and recombinant murine GM-CSF (Peprotech), respectively. Mϕ and DCs were infected with WNV-NY at an MOI of 0.01 and 0.001, respectively.

***(c) Cortical neurons*.** CN were prepared from the cerebral cortex of embryonic day 15 WT and *Ifi27l2a*$^{-/-}$ mice as described (42). Tissues were dissociated at 37˚C in 1 ml 0.25% (w/v)

trypsin, 0.25 mg DNase I (Sigma) in HBSS for 20 min. Trypsin was neutralized with 10% HI-FBS in DMEM and cells were filtered through a 70 μm filter and seeded at 5 x 10^5 cells/well on poly-D lysine and laminin (10 μg/ml)-coated 24-well cell-culture treated plates. CN cells were cultured in Neurobasal medium (Life Technologies) supplemented with 2% B-27 (Gibco), 1% Glutamax and 100 U/ml penicillin and streptomycin.

(d) Granule cell neurons. GCN were prepared from the cerebellum of 7 day-old pups and dissociated using the same protocol as for CN. These cells were cultured in the same medium as CNs with the addition of 40 mM KCl. Medium changes (50% of starting volume) were performed every 2 to 3 days, and neurons were maintained for 21 days in culture. In some experiments, neurons were pretreated for 24 h with 100 U/ml of IFN-β. Neurons were infected for 1.5 h at 37˚C, rinsed with HBSS twice and cultured in their respective complete neuronal medium. GCN were infected with WNV-NY or WNV-MAD at an MOI of 0.01 or 0.1, respectively. In some experiments, GCN were pretreated with IFN-β (150 or 100 IU/ml, for WNV-NY or WNV-MAD, respectively) for 24 h. Viral titer was determined by focus-forming assay, as previously described (43).

The purity of cultured neuron populations was defined by immunofluorescence microscopy analysis after incubating with antibodies to S100-β (1:200 dilution, Abcam 52642), NeuN (1:100 dilution, Milipore MAB377B), or IbaI (1:500 dilution, WAKO 019-19741) to identify astrocytes, neurons or microglia, respectively. Secondary Alexa fluor conjugated dyes 488 or 555 were used (1:400 dilution, Invitrogen) for detection. Samples were imaged with a Nuance FX multiplex biomarker imaging system (Perkin Elmer). Using this analysis, our GCN cultures were comprised of 85% neurons and 12% astrocytes.

Cytokine and chemokine profiling. Cytokines and chemokines were profiled from serum at days 4 and 6 after peripheral WNV-NY infection. Protein levels were assayed with Bio-Plex Pro Cytokine Assay per the manufacturer's protocol.

Immune cell analysis. Splenocytes and peripheral blood mononuclear cells were harvested from WT and *Ifi27l2a*$^{-/-}$ mice at day 8 after subcutaneous infection with WNV. Cells were stained for the following surface antigens following a 10 min preincubation with Fc-block (1:25 dilution; eBioscience): CD3 (1:25 dilution; BD Horizon, 500A2), CD4 (1:100 dilution; BioLegend, RM4-5), CD8α (1:100 dilution; Biolegend, 53-6.7), and CD19 (1:100 dilution; BioLegend, 6D5). Dead cells were excluded from analysis using Viability Dye eFluor (1:300 dilution; eBioscience). Cells were washed, fixed, permeabilized and stained for granzyme B (1:50 dilution; Invitrogen, GB11) and the APC-conjugated D^b-restricted NS4B peptide (SSVWNATTAI) tetramer (1:300 dilution, NIH Tetramer Facility (Atlanta, GA)). Blood monocytes were detected after staining with Gr-1 (1:100 dilution; BioLegend, RB6-8C5), CD115 (1:100 dilution; eBioscience AFS98), CD8α (1:100 dilution), and F4/80 (1:100 dilution; Serotec, CI:A3-1) antibodies. $CD8^-$ $CD115^+$ $F4/80^+$ cells were designated as monocytes after extensive gating analysis (44). The monocytes in blood include circulating $CD115^+$ $F4/80^+$ $Gr\text{-}1^{lo}$ monocytes that likely do not become resident within tissues. Circulating $CD115^+$ $F4/80^+$ $Gr\text{-}1^{hi}$ monocytes may enter tissue during inflammation ("inflammatory monocytes") and differentiate into macrophages (44-47). All samples were processed on a LSR Fortessa and data were analyzed by FlowJo software (Tree-Star).

CNS leukocytes were isolated according to a published method (48). Briefly, eight days following subcutaneous WNV infection, mice were perfused extensively with PBS. Brain tissue was minced, and digested in HBSS supplemented with 0.05% collagenase D (Sigma), 0.1 μg/ml trypsin inhibitor TLCK (N-α-p-tosyl-L-lysine chloromethyl ketone), 10 μg/ml DNase I (Sigma), and 10 mM HEPES, pH 7.3 for 30 min. CNS cells were strained with a 70 μm filter and subjected to Percoll gradient (30% v/v) purification (1,200 x g, 30 min). Cells were washed, incubated with Fc-block, and stained for CD8α (1:100 dilution), CD11b (1:100 dilution), CD19 (1:100 dilution), CD45 (1:100 dilution), Viability Dye eFluor (1:300 dilution) for 1 h at 4˚C, then

rinsed, and incubated with commercial cell fixative (eBioscience). Samples were processed on an LSR Fortessa flow cytometer and analyzed with FlowJo commercial software (Tree-Star). Neutrophils ($CD11b^{high}$ $CD45^{high}$) were identified by their unique high side scatter profile. Mϕ ($CD11b^{high}$ $CD45^{high}$) and microglial ($CD11b^{high}$ $CD45^{low}$) populations were identified by their relative expression of CD11b and C45 and their low to medium side scatter profiles.

The T_{FH} and germinal center B cell responses were measured in the draining lymph node (DLN) 8 days post infection with WNV-NY. Cells were stained as previously described with fluorochrome or biotin-conjugated antibodies purchased from BD Biosciences, Biolegend, and eBioscience: CD3ε (145-2C11), CD4 (RM4-5), CD19 (1D3), PD1 (29F.1A12), FAS (Jo2), GL7 and CXCR5 (2G8) (49).

Serum antibody analysis. WNV-specific IgG and IgM dilution endpoint titers were determined by ELISA against purified WNV E protein, as previously described (50). Focus reduction neutralization (FRNT50) assays were performed as previously described on Vero cells following serial dilution of serum with 100 FFU of WNV (39, 49).

TUNEL staining. Brain tissue was harvested from mice nine days after subcutaneous WNV infection. Mice were perfused with 30 ml PBS and half of the brain was retained for viral titer analysis, while the other brain half was fixed in 4% paraformaldehyde (PFA) in PBS overnight. This was followed by a 6 h incubation of brains in 20% sucrose solution and overnight incubation in 30% sucrose solution, all at 4˚C. Selected brains (from WT or *Ifi27l2a*$^{-/-}$ mice) with equivalent viral titers (1 to 8 x 10^5 PFU/g) were embedded in Optimal Cutting Temperature medium (OTC; Tissue-Tek), frozen at -80^{o}C, and sectioned in 10 μm slices on a Microm HM505N Cryostat on positively charged slides (Globe Scientific, 1358W). TUNEL staining was performed with the Roche *In Situ* Cell Death Detection Kit-TMR red per the manufacturer's instructions. Neurons were co-stained with anti-NeuN (1:100 dilution; Millipore, A60), secondary Alexa Fluor 488 (1:400 dilution) and nuclei were visualized with DAPI. Slides were mounted with

Prolong Gold Diamond anti-fade mounting media (Invitrogen). Tissues were imaged on a Zeiss LSM880, AxioObserver confocal microscope at the Washington University Microscopy Core Facility, with a Plan-Apochromat 40x/1.4 oil DIC M27 objective. DAPI, Alexa Fluor 488, and TMR-red were detected with the respected wavelength channels: 415-470, 491-553, and 553-624. The image, approximately 637.64 μm x 637.64 μm, was comprised by automated tiling of 9 panels (Zeiss Zen), with the central panel being selected for TUNEL positive cells in the same region of the brain tissue in each animal. Four mice were imaged per genotype with two tissue slices per mouse and two images per tissue slice for both brain stem and cerebellum. TUNEL positive events were counted within the 9-tiled composite image.

qRT-PCR assays. WNV, *Oas1a* and *Ifit1* mRNA was analyzed from RNA extracted from GCN following treatment with either IFN-β (100 U/ml), poly(I:C) (50μg/ml) (InvivoGen), WNV-NY (MOI, 5) or WNV-MAD (MOI, 5) for 8 h prior to collection in lysis buffer. qRT-PCR was performed as previously described for WNV, *Oas1a* and *Ifit1* and gene expression was normalized to *Gapdh* (51). Commercially available *Ifi27l2a* primer-probe assay was purchased from IDT. TaqMan RNA-to-C_T 1-Step Kit was used for qRT-PCR.

Blood-brain barrier permeability. Blood-brain barrier (BBB) studies were performed as previously described (52). Briefly, 4 days after subcutaneous infection with WNV-NY, WT and *Ifi27l2a*$^{-/-}$ mice were injected via an intraperitoneal route with 100 μl of a 100 mg/ml fluorescein (Sigma) in PBS. Dye was allowed to circulate for 45 min, serum was collected as a normalization control, mice were perfused with 20 ml PBS, and brain regions were collected for analysis as previously described (52).

Statistical analyses. All data were analyzed with Prism software (GraphPad Prism, San Diego, CA). qRT-PCR with more than two comparisons between groups was analyzed by one-way ANOVA with Tukey's HSD *post hoc* analysis. qRT-PCR data with two group comparisons was analyzed by Student's *t*-test with correction for multiple comparisons Holm-Sidak method.

Serum cytokine levels were analyzed by Student's *t*-test with correction for multiple comparisons Holm-Sidak method. Kaplan-Meier survival curves were analyzed by the Mantel-Cox Log-rank test. Viral burden in tissues was analyzed by the Mann-Whitney test. Serum antibody titers were analyzed by Student's *t*-test. For viral growth kinetics in cell culture, the log transformed viral titer was analyzed by Student's *t*-test. Flow cytometry based assays, where total cell count or percent total cell count was measured, also was analyzed by a Student's *t*-test.

RESULTS

A deficiency of *Ifi27l2a* increases susceptibility to WNV infection. The ISG *Ifi27l2a* is differentially upregulated in selected neurons of the brain after WNV infection, and ectopic expression of *Ifi27l2a* in cultured cortical neurons inhibited infection by WNV (14). To explore an antiviral role *in vivo* for this relatively poorly characterized ISG, we generated *Ifi27l2a*$^{-/-}$ mice using a targeted gene deletion strategy (**Fig 1A**); deletion of *Ifi27l2a* was validated by PCR (**Fig 1B**). In WT mice, basal *Ifi27l2a* mRNA expression was observed in lymph node, heart, lung and testes, and to a lesser extent in the kidney and spleen. Following WNV infection, *Ifi27l2a* mRNA expression was induced in the brain and spinal cord (**Fig 1C**). To quantify *Ifi27l2a* mRNA expression in response to viral infection, we analyzed selected tissues at successive time points following peripheral inoculation (**Fig 1D**). At 4 and 8 days post infection, *Ifi27l2a* mRNA expression was enhanced in the brain (2.0- and 3.3-fold, respectively; $P < 0.005$) and the spinal cord (2.1- and 2.0-fold, respectively; $P < 0.005$). Within the spleen, higher levels of *Ifi27l2a* mRNA were observed 4 days after infection (12-fold, $P < 0.05$). We also analyzed *Ifi27l2a*$^{-/-}$ and wild-type (WT) mice for possible differences in immune cells subsets in the spleen and blood. Although the numbers of $CD4^+$ and $CD8^+$ T cells and $CD19^+$ B cells were similar, *Ifi27l2a*$^{-/-}$ mice had slightly greater numbers of splenic NK cells ($NK1.1^+$) than WT mice (**Table 1**); while noteworthy, this phenotype may less important in the context of WNV infection, as NK cell depletion does not impact WNV pathogenesis in mice (53, 54). Within the peripheral blood leukocyte compartment, we observed similar numbers of myeloid cells, monocytes, and subsets of granulocytes (**Table 2**).

We next infected WT and *Ifi27l2a*$^{-/-}$ congenic mice with a pathogenic isolate of WNV (strain 3000.0259, WNV-NY). After subcutaneous infection with 10^2 PFU of WNV-NY, *Ifi27l2a*$^{-/-}$ mice exhibited a decreased survival rate compared to WT animals (29% versus 63%, $P < 0.05$) although the mean time to death was similar between the two groups (**Fig 2A**).

WNV burden in the CNS of *Ifi27l2a*$^{-/-}$ mice. To understand why an absence of *Ifi27l2a* resulted in enhanced pathogenicity of WNV-NY, viral burden was examined at different days (2, 4, 6, 8, 10, or 14) in serum, peripheral organs (spleen and kidney), and CNS tissues (brain and spinal cord). WNV viremia at days 2, 4, and 6 was similar between WT and *Ifi27l2a*$^{-/-}$ mice (**Fig 2B**). At all time points tested, viral burden in the spleen also was similar between WT and *Ifi27l2a*$^{-/-}$ mice (**Fig 2C**). Moreover, a deficiency in *Ifi27l2a* did not result in productive infection of the kidney (**Fig 2D**), an organ that is typically resistant to WNV-NY infection in WT mice yet permissive in animals with defects in type I IFN induction, signaling, or effector functions (55-59). However, within the CNS at day 8 after infection, WNV-NY burden increased in the brain (2.4-fold, $P < 0.05$) and spinal cord (170-fold increase, $P < 0.005$) of *Ifi27l2a*$^{-/-}$ mice (**Fig 2E and F**). This difference in viral titer was not apparent at later time points, and by day 14, infectious virus was not detectable within the CNS or peripheral tissues in surviving animals from both genotypes, suggesting that *Ifi27l2a*$^{-/-}$ animals did not have a defect in the clearance phase of WNV, which requires CD8^{+} effector T cells (36).

To corroborate these findings, we performed plaque assays on tissue homogenates isolated from specific regions of the CNS. WT and *Ifi27l2a*$^{-/-}$ mice were infected with WNV-NY via a subcutaneous route and viral burden in the brain stem, cerebellum, cerebral cortex, sub-cortex (defined in Methods), and olfactory bulb was measured at day 8 after infection (**Fig 2G-K**). Although we observed no differences in WNV titers in the cerebral cortex, sub-cortex, or olfactory bulb, higher levels of infection were observed in the cerebellum and brain stem (590-fold, $P < 0.05$; 5,200-fold, $P < 0.05$, respectively) from *Ifi27l2a*$^{-/-}$ mice. These data suggest that Ifi27l2a has a protective, antiviral role in selected regions of the CNS.

WNV infection after direct intracranial inoculation. As *Ifi27l2a*$^{-/-}$ mice exhibited higher viral titers in the brain stem and cerebellum, we postulated that Ifi27l2a might protect specific regions when virus was administered directly into the CNS. Unexpectedly, following intracranial inoculation of WNV-NY into the cerebral cortex, we observed no differences in viral titers within

different regions of the CNS at either 3 or 5 days after infection (**Fig 3A-F**). Because WNV-NY strain is highly virulent, we repeated intracranial infection studies with the attenuated WNV Madagascar strain (WNV-MAD), which is more sensitive to the antiviral effects of type I IFN (14, 37, 60). We observed a modest, (17-fold, $P < 0.05$) yet statistically significant phenotype, with greater WNV-MAD infection at day 3 after infection in the brain stem of *Ifi27l2a*$^{-/-}$ mice (**Fig 3G-L**). Thus, Ifi27l2a had an antiviral effect when virus was introduced directly into the CNS, although its magnitude was limited and only apparent with an attenuated, more IFN-sensitive strain.

Ifi27l2a does not alter cellular or humoral immune responses during acute WNV infection. As depressed antiviral CD8$^+$ T cell or antibody responses can facilitate dissemination to and replication of WNV within the CNS (reviewed in, 12), we investigated whether an absence of Ifi27l2a influenced the development of cellular and adaptive immunity during WNV-NY infection. Initially, we examined the effects of Ifi27l2a on lymphocyte numbers in the peripheral tissues. At baseline, normal numbers and percentages of B cells, CD4$^+$ T cells, and CD8$^+$ T cells were present in the blood and spleen. Because a previous study suggested that Ifi27l2a modulates inflammation, possibly through regulation of Mϕ differentiation (24, 35), we profiled monocytes in blood during WNV infection (**Fig 4A**). At day 8 after infection, *Ifi27l2a*$^{-/-}$ and WT mice had similar percentages and numbers of circulating and inflammatory blood monocytes based on differential expression of the surface markers F4/80, CD115, and Gr-1 (Ly6C and Ly6G) (**Fig 4B-C** and **Methods**).

We next evaluated T cell responses in peripheral organs by characterizing the relative levels of CD4$^+$ and CD8$^+$ T cells (**Fig 5A**). At day 8 after WNV-NY infection, equivalent percentages and numbers of CD4$^+$ and CD8$^+$ cells were observed in the spleen (**Fig 5B-C**). Furthermore, no difference in granzyme B$^+$ NS4B tetramer$^+$ antigen-specific CD8$^+$ T cells was observed in the spleens of WT and *Ifi27l2a*$^{-/-}$ mice. We assessed whether leukocyte accumulation in the CNS was altered, which independently could affect disease outcome.

Leukocytes were isolated from brains of WT and *Ifi27l2a*$^{-/-}$ mice at day 8 and analyzed by flow cytometry (**Fig 5D**). We observed similar percentages and numbers of CD4^{+} and CD8^{+} T cells or granzyme B^{+} NS4B tetramer^{+} CD8^{+} T cells within the brain (**Fig 5E-F**). Microglia and infiltrating Mϕ were characterized by CD45 and CD11b surface expression (**Fig 5G**). We also observed no differences in the percentage or numbers of activated microglia (CD11b^{high} CD45^{low}) or Mϕ (CD11b^{high} CD45^{high}) (**Fig 5H-I**) in the brains of WT and *Ifi27l2a*$^{-/-}$ mice after WNV-NY infection. Thus, a deficiency of Ifi27l2a did not affect priming, the recruitment, or activation of antigen-specific or innate immune cells in the CNS of WNV-infected mice.

To assess the effect of Ifi27l2a on WNV-specific antibody responses, we analyzed serum from *Ifi27l2a*$^{-/-}$ and WT mice on day 8 after infection for binding to the WNV E protein**.** We observed elevated IgG titers (3.2-fold, $P < 0.0005$) in *Ifi27l2a*$^{-/-}$ mice compared to WT mice (**Fig 6A**), but no difference in IgM titers (**Fig 6B**). However, neutralization assays detected no difference in the ability of serum-derived antibody from WT and *Ifi27l2a*$^{-/-}$ mice to neutralize WNV-NY infection (**Fig 6C**).

Because of the increased IgG titers in *Ifi27l2a*$^{-/-}$ mice, we next characterized whether there were differences in the T cell-dependent germinal center response in DLN of WNV-NY infected mice at 8 days post infection. T follicular helper cells were characterized as CD4^{+}, PD1^{+}, and CXCR5^{+} **(**T_{FH}, **Fig 6D)** and germinal center B cells were classified as CD19^{+}, Fas^{+}, and GL7^{+} **(**GC B, **Fig 6E)**. As the total numbers and percentages of T_{FH} and GC B cells were similar in WNV-infected WT and *Ifi27l2a*$^{-/-}$ mice, a deficiency in Ifi27l2a did not appear to alter the germinal center response within the DLN.

Cytokine and chemokine expression profiles in serum of WNV-infected *Ifi27l2a*$^{-/-}$ mice. Because specific vasoactive cytokines (e.g., TNF-α, IL-1β, and IL-6) can alter the blood-brain barrier (BBB) and affect transit of WNV into the brain parenchyma and early replication (reviewed in 10, 11), we measured whether a deficiency of Ifi27l2a affected systemic production

of cytokines and chemokines at 4 or 6 days after WNV-NY infection. In WNV infected mice, we observed greater expression of IL-1β and eotaxin in WT mice compared to *Ifi27l2a*$^{-/-}$ at 4 days after infection (3.0-fold, $P < 0.05$; 1.2-fold, $P < 0.05$), but not other cytokines and chemokines (**Table 3**). Consistent with this small variation in cytokine expression in serum, we did not observe differences in blood-brain barrier permeability between WT and *Ifi27l2a*$^{-/-}$ mice (data not shown). To assess whether this small variation in cytokine expression in serum impacted BBB permeability and possibly virus entry into the CNS, we injected the small molecule sodium fluorescein via an intraperitoneal route into WT and *Ifi27l2a*$^{-/-}$ at 4 days after WNV infection and then measured extravasation into different regions of the CNS. Notably, similar levels of sodium fluorescein accumulated in the cerebral cortex, cerebellum, brain stem, and spinal cord (data not shown). Thus, the small increases in serum cytokine levels in the absence of Ifi27l2a did not substantively impact BBB permeability.

Ifi27l2a exhibits antiviral effects against WNV in Mϕ but not DCs or MEFs. Although *Ifi27l2a* is expressed after WNV infection in primary and secondary lymphoid tissues, we did not observe greater viral burden in peripheral organs. We speculated that the antiviral effect of Ifi27l2a against WNV infection might not occur in non-neuronal cell types. To evaluate this hypothesis, we generated bone marrow-derived Mϕ and DCs and primary MEFs from WT and *Ifi27l2a*$^{-/-}$ mice. Cells were either pretreated with IFN-β or not treated and were then subsequently infected at a low MOI with WNV-NY. We observed increased WNV-NY replication in untreated or IFN-β treated Mϕ at later time points ($P < 0.05$, **Fig 7A**). However, we observed no difference in viral infection at any time point in DC or MEF cultures generated from WT and *Ifi27l2a*$^{-/-}$ mice (**Fig 7B-C**).

Subsets of primary neurons from *Ifi27l2a*$^{-/-}$ mice exhibit enhanced WNV infection. Given that the virologic phenotype occurred in selected brain regions of *Ifi27l2a*$^{-/-}$ mice, we investigated whether Ifi27l2a had differential antiviral activity in different neuron populations. We

prepared primary neurons from the cerebral cortex (CN) and cerebellum (GCN) of WT and *Ifi27l2a*$^{-/-}$ mice, pretreated select cells with IFN-β, and measured viral growth kinetics after infection with WNV-NY. We detected no differences in replication kinetics in CN, with only mild suppression of infection with IFN-β pretreatment (**Fig 8A**), as seen previously (14). Somewhat unexpectedly, we observed similar viral growth kinetics in GCN from WT and *Ifi27l2a*$^{-/-}$ mice for WNV-NY, with replication being suppressed to a greater degree following IFN-β pretreatment (**Fig 8B**), also as reported previously (14). We reassessed viral growth kinetics with the more IFN-sensitive strain, WNV-MAD. *Ifi27l2a*$^{-/-}$ GCN supported higher levels of WNV-MAD infection and this effect was more pronounced when cells were pretreated with IFN-β (18-fold, $P < 0.05$, **Fig 8C**) and a difference in viral replication was present in non-IFN-β treated cells (55-fold). Consistent with this data, by 72 hours after infection, a greater proportion of WNV-MAD infected GCN was observed in *Ifi27l2a*$^{-/-}$ versus WT GCN (**Fig 8D**). Because we observed differences in WNV restriction in WT and *Ifi27l2a*$^{-/-}$ GCN, we considered whether a deficiency of Ifi27l2a altered the general ISG response in GCN. We treated cells with known ISG inducers (IFN-β, Poly(I:C), WNV-NY and WNV-MAD) and assessed expression of *Oas1a* and *Ifit1* mRNA. As *Oas1a* and *Ifit1* induction was similar in WT and *Ifi27l2a*$^{-/-}$ GCN (**Fig 8E-F**), a deficiency of Ifi27l2a did not broadly impact expression of other antiviral ISGs.

***Ifi27l2a*$^{-/-}$ mice exhibit less neuronal death in the cerebellum and brain stem after WNV infection.** To provide a mechanistic link between our *in vitro* and *in vivo* phenotypes with *Ifi27l2a*$^{-/-}$ cells and mice, we prepared brain tissue sections for histological and immunohistochemical analyses. Although historically we have detected WNV antigen staining in neurons of different brain regions at day 9 after infection in younger (e.g., 5 and 8 week-old mice) (61, 62), despite multiple attempts, the viral antigen staining in 11 to 12 week-old WT or *Ifi27l2a*$^{-/-}$ mice was inconclusive. The levels of viral antigen in the CNS were at the threshold of detection, with only sporadic staining of infected neurons in different brain regions of a subset of the mice (data not shown). Because of this, and prior reports suggesting that some Ifi27 family

429 members (e,g., ISG12a) were required for IFN-induced cellular apoptosis (21, 31, 32), we
430 evaluated neuronal cell death in WT and *Ifi27l2a*$^{-/-}$ mice that had equivalent WNV titers in the
431 brain at 9 days after infection. We noted significantly more cell death in the cerebellum (5-fold, P
432 < 0.05) (**Fig 9A and C**) and brain stem (4-fold, P < 0.005) (**Fig 9B and C**) of WT mice, whereas
433 TUNEL positive neurons were largely absent in the hindbrain regions of *Ifi27l2a*$^{-/-}$ mice.
434

435 **DISCUSSION**

436 Viral replication and the subsequent immune response within the CNS can result in
437 significant morbidity and mortality. Because neurons are largely non-renewable, it is imperative
438 that the host clears viral infection while protecting cells from direct or collateral immune-
439 mediated damage. We previously identified *Ifi27l2a* as a putative inhibitory ISG that was
440 expressed preferentially within neurons of the cerebellum compared to those from the cerebral
441 cortex (14). Here, we established a protective antiviral role for Ifi27l2a *in vivo* against WNV.
442 *Ifi27l2a*$^{-/-}$ mice were more susceptible to WNV-induced mortality, and sustained higher viral titers
443 in the cerebellum, brain stem, and spinal cord. Remarkably, at day 9 after infection, *Ifi27l2a*$^{-/-}$
444 mice had less cell death in neurons of the cerebellum and brain stem. *Ifi27l2a*$^{-/-}$ mice showed no
445 apparent defects in their ability to generate peripheral or CNS cellular immune response, and
446 WNV replication was equivalent in several other cell types that lacked or expressed Ifi27l2a.

447 Several members of the Ifi27 family have been studied in the context of viral infections.
448 Many viruses induce expression of Ifi27 family members, including influenza A virus, Sindbis
449 virus, WNV, JEV, and human immunodeficiency virus-1 (14, 63-66). Our prior study reported
450 that ectopic expression of *Ifi27l2a* in CN reduced WNV infection whereas siRNA mediated gene
451 silencing in GCN resulted in enhanced viral replication (14). Work by others has shown that
452 ectopic expression of human *IFI27* (*ISG12A*) inhibited replication of HCV in Huh-7.5 cells, and
453 reciprocally siRNA mediated silencing of human *IFI27* enhanced HCV replication (67). High
454 levels of expression of human *IFI27* also inhibited Newcastle Disease virus (NDV) replication
455 and oncolytic activity in Huh7 cells (34).

456 *Ifi27l2a*$^{-/-}$ mice have been investigated in other contexts. Although *Ifi27l2a* was identified as
457 an upregulated ISG in lung tissue following influenza virus infection (65), *Ifi272la*$^{-/-}$ C57BL/6 mice
458 did not sustain higher viral burden or altered pathology in the lungs of infected animals (33). In
459 another *Ifi27l2a*$^{-/-}$ mouse of mixed genetic background, gene-deficient animals were protected
460 against caecal ligation induced-sepsis, LPS endotoxemia, or vascular injury after arterial ligation

(24, 35). In contrast, our *Ifi27l2a*$^{-/-}$ C57BL/6 mice succumbed to LPS administration at a rate similar to WT mice (T. Lucas and M. Diamond, unpublished observations). Although *Ifi27l2a* has a postulated role in regulating inflammation, at least in the context of WNV infection, we failed to observe hypercytokinemia, changes in the infiltrating immune cells, or altered adaptive immunity in *Ifi27l2a*$^{-/-}$ mice.

The unique cell-type expression, sub-cellular localization, and induction patterns of Ifi27 family genes suggest possible modular functions. Humans have four IFI27 members, of which only *IFI27* and *IFI6-16* (*IFI6*) are IFN-inducible. Mice have three gene paralogs, *Ifi27* (*Ifi27l1*), *Ifi27l2a,* and *Ifi27l2b*, all of which are IFN-inducible, with *Ifi27l2a* exhibiting the greatest induction after type I IFN treatment (19). IFI27 family members have been suggested to localize to the mitochondria (21, 22) or to the nuclear membrane (23, 24); in the latter case, IFI27 interacts with and sequesters the nuclear receptor NR4A1, which regulates expression of anti-inflammatory genes (24). IFI27 family members also appear to have pro-apoptotic effects (21, 32, 34, 68, 69), possibly through stabilization of the mitochondrial membrane and regulation of caspase activity (21, 68). Perhaps because of these proposed pleotropic activities, IFI27 family members have been associated with over-expression in certain cancers (69, 70), promotion of skin keratinocyte replication (71), and DNA-damage induced apoptosis and cytochrome c release (21). *IFI6-16* (*IFI6*) is an ISG12-motif containing family member that may share some functions with *Ifi27l2a*. In the context of DENV infection, a deficiency of IFI6-16 was associated with increased caspase levels and decreased Bcl-2 expression and mitochondrial membrane stabilization (68). Additionally, ectopic expression of *IFI6-16* has been shown to suppress infection of YFV virus (72). Our *in vivo* data is most consistent with a model in which Ifi27l2a is induced by type I IFN in response after WNV infection, and in a cell-type specific manner (for reasons that still remain uncertain), promotes cell death. In its absence (*Ifi27l2a*$^{-/-}$ mice), subsets of virally infected neurons (e.g., in the cerebellum, brain stem, and possibly spinal cord) live longer, which allows greater yields of virus to accumulate, at least during the early phase of

CNS infection. We speculate that the increased rate of death of WNV-infected Ifi27l2a$^{-/-}$ mice ultimately is caused by virus-induced injury of neurons in regions of the CNS that control key or autonomic function. Our study, along with the work of others, suggest multiple possible functions for different Ifi27 family members, with some of the antiviral properties being linked to cell death phenotypes in infected cells.

The predominant effect of Ifi27l2a in the CNS suggests a specialization of the host antiviral immune response. Analogously, preferential antiviral roles in the CNS for other ISGs (*Ifit2* and *Rsad2* (viperin)) have been reported. In *Ifit2*$^{-/-}$ mice, higher WNV and VSV titers were observed in the olfactory bulb, brain stem, and cerebellum (13, 73). In *Rsad2*$^{-/-}$ mice, an increase in WNV infection was observed in the cerebral cortex, white matter, and spinal cord (55). We observed differences in the regional restriction of WNV in the CNS mostly in the context of peripheral viral but not intracranial infection, with the exception of the brain stem. Viral infection of peripheral immune tissues (e.g., lymph node or spleen) may induce systemic accumulation of type I IFN that primes the antiviral response in the brain either earlier or prior to viral entry into the CNS, whereas direct administration of virus to the CNS may permit rapid replication of WNV in neurons in the context of a less robust type I IFN response. Although future studies are needed to determine why region-specific antiviral effects of individual ISGs occur, we speculate that these genes do not function in isolation, and partner proteins that are expressed differentially may regulate their activity. While our findings suggest an antiviral function within select neurons and Mϕ, the precise cellular mechanism of action of Ifi27l2a warrants further investigation.

In summary, we have identified a protective role for Ifi27l2a in the CNS following WNV infection. Ifi27l2a mediated restriction of WNV was greatest in the cerebellum, brain stem and spinal cord, and correlated with an antiviral and cell survival effect in subsets of neurons and myeloid cells. These findings suggest that Ifi27l2a may have a discrete antiviral activity within selected regions of the CNS.

513 **ACKNOWLEDGEMENTS**

514 National Institutes of Health (NIH) grants U19 AI083019, U19 AI106772, R01 AI104972,
515 and R01 AI104002 supported this study. T.M.L. and J.M.R. were supported by NIH-NRSA
516 grants 5T32AI007172-33 and 5F32AG043223-02, respectively. We would like to thank A. Pinto
517 and J. Miner for help with the serum cytokine and BBB experiments, J. Williams and G.
518 Randolph for advice on monocyte gating and analysis, M. Ilagan at the Washington University
519 High Throughput Screening Core for assistance with the high content imaging and analyses,
520 and W. Beatty and B. Anthony at the Washington University Microscopy Core for assistance
521 with confocal imaging.

522

523

524 **FIGURE LEGENDS**

525 **Figure 1. Generation of *Ifi27l2a*$^{-/-}$ mice and tissue expression of *Ifi27l2a*.** Scheme of
526 Ifi27l2a locus with targeting cassette (**A**). Exons are noted in grey and target location is noted
527 with black arrow. *Ifi27l2a* gene deletion was verified by PCR. Genotyping was verified with a
528 positive control plasmid containing wild-type *Ifi27l2a* and negative controls with a null plasmid
529 control. *Ifi27l2a* deletion was confirmed by the presence of 408 bp band, whereas WT *Ifi27l2a*
530 manifests as a 612 bp band (**B**). The *Ifi27l2a* RT-PCR product was screened for in brain, spinal
531 cord, lymph node (LN), spleen, kidney, lung, liver, white fat, and testes (**C**). Selected mice were
532 infected subcutaneously with WNV-NY and tissues were collected 4 days after infection and
533 compared to mock-infected animals. The results are representative of 2 to 3 mice per treatment
534 group. Following peripheral infection by WNV-NY, selected tissues were collected at 4 and 8
535 days after infection and expression of *Ifi27l2a* mRNA was compared to mock infected animals
536 (**D**). *Ifi27l2a* mRNA was measured in brain, spinal cord, spleen, and lymph node, and
537 normalized to *Gapdh* by qRT-PCR. Means were compared between mock and infected groups
538 using one-way ANOVA followed by Tukey's HSD *Post Hoc* analysis (*, $P < 0.05$, **, $P < 0.005$).
539 Bars are mean $\pm$ SEM.

540 **Figure 2**. **Survival and viral burden analysis for WT and *Ifi27l2a*$^{-/-}$ mice infected**
541 **with WNV.** (**A**) Survival analysis of 11 to 12 week-old WT or *Ifi27l2a*$^{-/-}$ mice after inoculation with
542 10^2 PFU of WNV-NY by subcutaneous injection in the footpad. In (**A**) WT (n = 39) and *Ifi27l2a*$^{-/-}$
543 (n = 34) mice were used for survival curves. Asterisks indicate differences that were statistically
544 significant compared to WT mice (Mantel-Cox log rank test analysis; $P < 0.05$). Viral burden
545 after WNV-NY infection of WT or *Ifi27l2a*$^{-/-}$ mice was measured by qRT-PCR (**B**) or plaque
546 assay (**C-G**) in samples from serum (**B**), Spleen (**C**), kidney (**D**), brain (**E**), and spinal cord (**F**) at
547 the indicated time points after infection. (**G-K**) Selected brain regions were assayed for viral
548 burden at 8 days post subcutaneous infection with WNV-NY. Data points represent individual
549 mice. Bars indicate median values and were obtained from 16 to 17 mice per tissue. Asterisks

indicate statistical significance as determined by the Mann-Whitney test (*, $P < 0.05$, **, $P < 0.005$). Dotted line indicates the limit of detection for each tissue. Data are pooled from at least three independent experiments.

Figure 3. Viral titers in the brain after intracranial infection of WT and *Ifi27l2a*$^{-/-}$ mice. Mice were infected with either 10^1 PFU WNV-NY (**A-F**) or WNV-MAD (**G-L**) via an intracranial route and selected CNS regions were harvested and viral burden was determined by plaque assay. Data points represent individual mice. Bars indicate median values and were obtained from 4 to 10 mice per time point per tissue. Dotted lines represent the limit of detection of the assay. Asterisks indicate statistical significance as determined by the Mann-Whitney test (*, $P < 0.05$).

Figure 4. Circulating monocytes isolated from the blood of WT and *Ifi27l2a*$^{-/-}$ mice. Circulating blood monocytes were gated as CD8$^-$ F4/80$^+$ CD115$^+$ and analyzed for expression of additional surface markers including Gr-1 (Ly6C and Ly6G) (**A**). WT and *Ifi27l2a*$^{-/-}$ monocytes were present at similar levels at 8 days post infection in the blood. Specific monocyte populations of Gr-1^{high} and Gr-1^{low} cells were phenotyped according to prior studies (45, 74) and presented as either percent (**B**) or total number (**C**) of cells per ml of blood from WT and *Ifi27l2a*$^{-/-}$ mice. For each group, a Student's *t*-test was used to compare cells from WT to *Ifi27l2a*$^{-/-}$ mice. Bars indicate mean values for 8 to 9 mice for each genotype from three independent experiments.

Figure 5. Splenic T cell and brain-specific immune response to WNV infection in WT and *Ifi27l2a*$^{-/-}$ mice. (**A**) T cells were identified by inclusion of CD19$^-$ and CD3$^+$ cells, and analyzed by CD4 and CD8. CD8$^+$ cells were additionally analyzed as granzyme B$^+$ and WNV-specific NS4B tetramer$^+$. At 8 days after subcutaneous infection with WNV-NY, splenocytes were harvested. Similar percentages (**B**) and absolute cell numbers (**C**) were observed for CD4$^+$ T cells, CD8$^+$ T cells or WNV specific granzyme B$^+$ NS4B tetramer$^+$ CD8$^+$ T cell ($n = 11$). For each group, Student's *t*-test was used to compare values from WT to *Ifi27l2a*$^{-/-}$ mice ($P < 0.05$).

Bars indicate mean values. Brain cells were purified by Percoll gradient centrifugation from brains of mice at 8 days post infection. (**D**) Cells were gated as $CD8^+$ positive, and WNV-specific $CD8^+$ T cells were identified by co-staining for granzyme B and with WNV-specific NS4B tetramer. The percentages of $CD4^+$ and $CD8^+$ T cells, as well as NS4B-specific cells, were similar between WT and *Ifi27l2a*$^{-/-}$ mice (**E**). No difference in absolute number of infiltrating $CD4^+$ and $CD8^+$ T cells, or the WNV specificity of $CD8^+$ T cells was observed (**F**). Brains were analyzed for numbers of macrophages ($CD45^{high}$ $CD11b^+$) and microglia ($CD45^{low}$ and $CD11b^+$) (**G**). The percentages and number (**H-I**) of macrophages and microglia were similar between WT and *Ifi27l2a*$^{-/-}$ mice. WT and *Ifi27l2a*$^{-/-}$ samples percentages and absolute numbers for three independent experiments were compared with a Student's *t*-test (n = 7 to 11 mice, *, $P < 0.05$). Bars indicate mean values. Y-axes are cell-type dependent.

Figure 6. **Antibody responses in WT and *Ifi27l2a*$^{-/-}$ mice after WNV infection.** Serum was obtained from WNV-infected WT and *Ifi27l2a*$^{-/-}$ mice and IgG levels (**A**) or IgM levels (**B**) at 8 days after infection and measured by ELISA for reactivity with WNV E protein. Neutralizing antibody titers were determined by a focus-reduction assay from serum at day 8 (**C**). Results are shown as a scatter plot and represent samples from 7 to 10 mice per group. Data are plotted as the $\log_{10}$ endpoint neutralization titer or $\log_{10}$ focus reduction neutralizing titer 50 (FRNT50). A Student's *t*-test was used to compare data from WT and *Ifi27l2a*$^{-/-}$ mice (***, $P < 0.0005$). **D-G**. T_{FH} cells ($PD1^+$ and $CXCR5^+$) **(D)** and GC B cells (Fas^+ and $GL7^+$) **(E)** populations were identified in the DLN at 8 days post WNV-NY infection. Total numbers of T_{FH} cells and GC B cells **(F)** and percentages of T_{FH} cells of total $CD4^+$ cells and GC B cells of total $CD19^+$ cells **(G)** were similar between WT and *Ifi27l2a*$^{-/-}$ mice. Bars indicate mean values.

Figure 7. Ifi27l2a restricts WNV replication in Mϕ, but not DC or MEFs. (**A**) Bone marrow derived Mϕ were infected with WNV (MOI, 0.01) and viral replication kinetics were followed for 72 h. A subset of Mϕ was pretreated with IFN-β (1 U/ml for 6 h) prior to infection. (**B**)

Bone marrow derived DCs were infected with WNV (MOI, 0.001) and viral kinetics were followed for 72 h. A subset of DCs was pretreated with IFN-β (10 U/ml for 6 h) prior to infection. (**C**) MEFs were infected with WNV (MOI, 0.01) and viral kinetics were followed for 72 h. A subset of MEFs was pretreated with IFN-β (10 U/ml for 6 h). The data analyzed by a Student's *t*-test for each time point, between each treatment group and is expressed as the $\log_{10}$ median titers ± SEM as reflects pooled data from 3 to 4 independent experiments with three technical replicates per independent experiment for each cell type. Y-axes range is cell-type dependent.

Figure 8. Viral infection of WT and *Ifi27l2a*$^{-/-}$ primary neurons. Primary neuron cultures were generated from WT and *Ifi27l2a*$^{-/-}$ mice and infected with WNV-NY or WNV-MAD Cell supernatants were harvested at the indicated time points and titrated by focus forming assay. CN (**A**) and GCN (**B-C**) were infected at the following MOI: WNV-NY, 0.01; WNV-MAD, 0.1. In some experiments, GCN and CN were pretreated with IFN-β for 24 h (CN: 150 U/ml for WNV-NY; GCN: 150 U/ml for WNV-NY or 100 U/ml WNV-MAD). **(D)** WT and *Ifi27l2a*$^{-/-}$ GCN were infected with WNV-MAD for 72 h and infected neurons (MAP2^{+}) cells were counted by automated high throughput imaging. WT and *Ifi27l2a*$^{-/-}$ GCN were analyzed by qRT-PCR for expression of *Oas1* (**E**) and *Ifit1* (**F**)**.** Viral replication data was analyzed at each time point, for each treatment by a Student's *t*-test for each treatment group (*, $P < 0.05$, $n = 3$ to independent replicates). GCN infection assay results were analyzed by Student's *t*-test (two experimental replicates, 3 to 4 samples wells per replicate) (*, $P < 0.05$). For high throughput imaging, three wells per treatment group were analyzed for each biological replicate (n = 3). For each well, 60 computer-randomized images were collected and analyzed by GE IN Cell 2000 imager and IN Cell Software. qRT-PCR data was analyzed by a Student's *t*-test with correction for multiple comparisons by Holm-Sidak method (*,$P < 0.05$). NT = Not treated.

Figure 9. Neuronal death within the cerebellum and brain stem of WNV infected mice. Nine days following subcutaneous infection with WNV-NY, brains of selected mice with

similar levels of virus were sectioned and stained for neurons (NeuN, green), cell death (as determined by TUNEL staining, red) and nuclei (DAPI, blue). Cerebellum **(A)** and brain stem **(B)** tissues were analyzed by confocal microscopy and fields of view containing TUNEL staining were quantitated for number of events per field of view **(C)** (n = 4 mice per genotype, 2 sections per mouse, 2 fields of view per section). The relative number of $TUNEL^+$ cells in WT and *Ifi27l2a*$^{-/-}$ mice were analyzed by Student's *t*-test, with bars indicating the means (*, $P < 0.05$; **, $P < 0.005$). Scale bars = 100 μm. Yellow arrows indicate examples $TUNEL^+$ nuclei.

634 **Table 1. Immunophenotyping of lymphocytes in the spleen of naive WT and *Ifi27l2a*$^{-/-}$**

635 **mice.**

		WT				Ifi27l2a$^{-/-}$			
		Absolute		Percent		Absolute		Percent	
Subset		**AVG**	**±SD**	**AVG**	**±SD**	**AVG**	**±SD**	**AVG**	**±SD**
CD4$^+$	-	2.84E+08	4.74E+07	14.20	1.78	2.95E+08	2.72E+07	14.13	1.08
	CD44^{high} CD62l^{low}	3.05E+07	2.26E+06	10.88	1.08	3.52E+07	8.57E+06	11.93	2.85
	CD44^{low} CD62l^{high}	2.10E+08	2.14E+08	73.60	2.68	4.22E+07	2.56E+07	72.39	5.09
CD8$^+$	-	2.01E+08	3.21E+07	10.04	1.06	2.05E+08	2.67E+07	9.79	0.62
	CD44^{high} CD62l^{low}	3.41E+06	6.46E+05	1.75	0.47	4.69E+06	2.19E+06	2.31	1.13
	CD44^{low} CD62l^{high}	1.93E+08	3.21E+07	96.20	0.94	1.95E+08	2.79E+07	94.93	2.77
CD19$^+$	-	1.36E+09	2.34E+08	69.26	2.65	1.40E+09	1.92E+08	67.86	2.63
	IgM^{high}	1.36E+09	2.34E+08	98.14	0.31	1.40E+09	1.92E+08	98.02	0.29
NK	-	4.93E+05*	8.21E+04	2.41*	0.30	7.46E+05*	1.17E+05	3.47*	0.21

636

637 Mean (AVG) ± standard deviation (SD) for cells from WT and *Ifi27l2a*$^{-/-}$ mice (n = 5 mice each, *,

638 $P < 0.05$). The percentage of indicated populations are calculated as a proportion of the total

639 parent population.

640
641

Table 2. Immunophenotyping of myeloid cells in peripheral blood of naïve WT and *Ifi27l2a*$^{-/-}$ mice.

		WT				Ifi27l2a$^{-/-}$			
		Absolute		Percent		Absolute		Percent	
Subset		**AVG**	**±SD**	**AVG**	**±SD**	**AVG**	**±SD**	**AVG**	**±SD**
Monocyte	-	2.31E+05	2.90E+04	7.54	0.52	2.72E+05	1.03E+05	8.98	2.50
	Gr-1^{high}	1.68E+05	2.60E+04	72.62	3.68	1.96E+05	9.22E+04	70.58	5.44
	Gr-1^{low}	6.17E+04	8.17E+03	26.90	3.73	7.49E+04	1.58E+04	29.04	5.48
Neutrophil	-	3.53E+05	1.30E+05	11.20	2.44	3.16E+05	9.53E+04	10.48	2.02
Eosinophil	-	3.07E+04	1.84E+04	0.96	0.41	3.02E+04	1.78E+04	0.99	0.47

Number of cells per ml blood (AVG) ± standard deviation (SD) from WT and Ifi27l2a$^{-/-}$ (n = 5) mice. The percentage of indicated populations are calculated as a proportion of the total parent population.

Table 3. Serum cytokine levels at days 4 and 6 after subcutaneous inoculation of WNV.

		4 dpi				6 dpi			
		WT		*Ifi27l2a*$^{-/-}$		WT		*Ifi27l2a*$^{-/-}$	
	LOD	MEAN	SD	MEAN	SD	MEAN	SD	MEAN	SD
IL-1α	4.66	6.4	4.7	4.6	0.8	5.4	1.3	4.7	0.0
IL-1β	32.95	182.2*	88.2	60.1*	44.0	53.2	43.6	78.9	145.8
IL-2	2.92	19.4	8.6	27.0	10.4	19.1	14.2	16.3	10.6
IL-3	1.32	4.7	2.6	2.8	1.4	2.9	1.0	1.9	1.2
IL-4	6.11	7.2	2.0	5.7	1.2	5.3	1.6	5.7	4.6
IL-5	1.76	91.8	190.4	23.1	6.1	29.9	20.8	22.1	12.0
IL-6	0.86	26.1	55.4	5.5	0.9	10.9	16.2	5.2	2.5
IL-9	26.47	26.5	0.0	26.5	0.0	26.5	0.0	26.5	0.0
IL-10	6.32	62.3	40.9	47.6	20.3	38.1	19.2	24.0	14.5
IL-12(p40)	1.7	229.5	114.9	179.2	54.0	151.5	46.4	134.2	27.2
IL-12(p70)	0.99	34.1	16.3	24.5	9.3	19.5	14.4	8.4	8.2
IL-13	63.51	212.9	54.2	162.3	57.9	178.0	57.6	144.8	18.7
IL-17	2.94	29.7	16.4	28.6	7.9	25.2	10.9	26.7	13.4
Eotaxin	38.95	454.6*	90.9	370.2*	157.6	371.8	125.7	379.5	138.4
G-CSF	4.11	39.5	13.6	26.4	8.7	36.7	11.9	16.8	6.8
GM-CSF	51.12	116.2	29.4	78.0	35.9	96.1	24.5	61.0	32.8
IFN-γ	1.55	5.7	1.6	4.6	1.5	3.9	1.9	3.3	1.3
KC	1.43	97.1	48.0	120.6	44.4	66.2	35.9	67.1	35.3
MCP-1	15.39	156.3	54.0	147.5	20.1	130.7	46.6	110.7	39.3
MIP-1α	1.76	11.2	2.6	10.9	1.3	9.8	2.0	8.6	2.4
MIP-1β	6.81	41.1	38.8	24.4	8.7	15.5	10.6	17.1	14.7
RANTES	0.81	34.6	8.1	32.5	12.6	33.8	10.9	37.4	15.4
TNF-α	3.01	148.2	110.4	97.7	27.5	98.6	33.5	82.9	21.5

Cytokine levels were assayed via Bioplex Pro to determine relative differences between WT and *Ifi27l2a*$^{-/-}$ mice (n = 8 to 9 mice per genotype per time point) at 4 and 6 days after infection of 10^2 FFU by subcutaneous route. Data is the mean ± standard deviation (SD). Levels were compared between WT and *Ifi27l2a*$^{-/-}$ by Student's t-test ($P < 0.05$), with correction for multiple comparisons with Holm-Sidak method. LOD = Limit of Detection for each cytokine based on manufacture's protocol for establishing standard curves for each parameter measured.

REFERENCES

1. **Carson PJ, Konewko P, Wold KS, Mariani P, Goli S, Bergloff P, Crosby RD.** 2006. Long-Term Clinical and Neuropsychological Outcomes of West Nile Virus Infection. Clinical Infectious Diseases **43:**723-730.
2. **Chan CK, Limstrom SA, Tarasewicz DG, Lin SG.** 2006. Ocular Features of West Nile Virus Infection in North America: A Study of 14 Eyes. Ophthalmology **113:**1539-1546.
3. **Leis AA, Fratkin J, Stokic DS, Harrington T, Webb RM, Slavinski SA.** 2003. West Nile poliomyelitis. The Lancet Infectious Diseases **3:**9-10.
4. **Hainline ML, Kincaid JC, Carpenter DL, Golomb MR.** 2008. West Nile Poliomyelitis in a 7-Year-Old Child. Pediatric Neurology **39:**350-354.
5. **Bigham AW, Buckingham KJ, Husain S, Emond MJ, Bofferding KM, Gildersleeve H, Rutherford A, Astakhova NM, Perelygin AA, Busch MP, Murray KO, Sejvar JJ, Green S, Kriesel J, Brinton MA, Bamshad M.** 2011. Host Genetic Risk Factors for West Nile Virus Infection and Disease Progression. PLoS ONE **6:**e24745.
6. **Glass WG, McDermott DH, Lim JK, Lekhong S, Yu SF, Frank WA, Pape J, Cheshier RC, Murphy PM.** 2006. CCR5 deficiency increases risk of symptomatic West Nile virus infection. The Journal of Experimental Medicine **203:**35-40.
7. **Lim JK, McDermott DH, Lisco A, Foster GA, Krysztof D, Follmann D, Stramer SL, Murphy PM.** 2010. CCR5 Deficiency Is a Risk Factor for Early Clinical Manifestations of West Nile Virus Infection but not for Viral Transmission. Journal of Infectious Diseases **201:**178-185.
8. **Lim JK, Lisco A, McDermott DH, Huynh L, Ward JM, Johnson B, Johnson H, Pape J, Foster GA, Krysztof D, Follmann D, Stramer SL, Margolis LB, Murphy PM.** 2009. Genetic Variation in *OAS1* is a Risk Factor for Initial Infection with West Nile Virus in Man. PLoS Pathog **5:**e1000321.
9. **Cho H, Diamond MS.** 2012. Immune Responses to West Nile Virus Infection in the Central Nervous System. Viruses **4:**3812-3830.
10. **Suen W, Prow N, Hall R, Bielefeldt-Ohmann H.** 2014. Mechanism of West Nile Virus Neuroinvasion: A Critical Appraisal. Viruses **6:**2796-2825.
11. **Neal JW.** 2014. Flaviviruses are neurotropic, but how do they invade the CNS? Journal of Infection **69:**203-215.
12. **Suthar MS, Diamond MS, Gale Jr M.** 2013. West Nile virus infection and immunity. Nat Rev Micro **11:**115-128.
13. **Cho H, Shrestha B, Sen GC, Diamond MS.** 2013. A Role for Ifit2 in Restricting West Nile Virus Infection in the Brain. Journal of Virology **87:**8363-8371.
14. **Cho H, Proll SC, Szretter KJ, Katze MG, Gale M, Diamond MS.** 2013. Differential innate immune response programs in neuronal subtypes determine susceptibility to infection in the brain by positive-stranded RNA viruses. Nat Med **19:**458-464.
15. **Nair S, Michaelsen-Preusse K, Finsterbusch K, Stegemann-Koniszewski S, Bruder D, Grashoff M, Korte M, Köster M, Kalinke U, Hauser H, Kröger A.** 2014. Interferon Regulatory Factor-1 Protects from Fatal Neurotropic Infection with Vesicular Stomatitis Virus by Specific Inhibition of Viral Replication in Neurons. PLoS Pathog **10:**e1003999.
16. **Farmer JR, Altschaefl KM, O'Shea KS, Miller DJ.** 2013. Activation of the Type I Interferon Pathway Is Enhanced in Response to Human Neuronal Differentiation. PLoS ONE **8:**e58813.
17. **Rosato PC, Leib DA.** 2014. Intrinsic Innate Immunity Fails To Control Herpes Simplex Virus and Vesicular Stomatitis Virus Replication in Sensory Neurons and Fibroblasts. Journal of Virology **88:**9991-10001.

18. **Yordy B, Iijima N, Huttner A, Leib D, Iwasaki A.** 2012. A Neuron-Specific Role for Autophagy in Antiviral Defense against Herpes Simplex Virus. Cell Host & Microbe **12:**334-345.
19. **Parker N, Porter A.** 2004. Identification of a novel gene family that includes the interferon-inducible human genes 6-16 and ISG12. BMC Genomics **5:**8.
20. **Cheriyath V, Leaman DW, Borden EC.** 2011. Emerging roles of FAM14 family members (G1P3/ISG 6-16 and ISG12/IFI27) in innate immunity and cancer. J Interferon Cytokine Res **31:**173-181.
21. **Rosebeck S, Leaman DW.** 2008. Mitochondrial localization and pro-apoptotic effects of the interferon-inducible protein ISG12a. Apoptosis **13:**562-572.
22. **Li B, Shin J, Lee K.** 2009. Interferon-Stimulated Gene ISG12b1 Inhibits Adipogenic Differentiation and Mitochondrial Biogenesis in 3T3-L1 Cells. Endocrinology **150:**1217-1224.
23. **Martensen PM, Søgaard TMM, Gjermandsen IM, Buttenschøn HN, Rossing AB, Bonnevie-Nielsen V, Rosada C, Simonsen JL, Justesen J.** 2001. The interferon alpha induced protein ISG12 is localized to the nuclear membrane. European Journal of Biochemistry **268:**5947-5954.
24. **Papac-Milicevic N, Breuss JM, Zaujec J, Ryban L, Plyushch T, Wagner GA, Fenzl S, Dremsek P, Cabaravdic M, Steiner M, Glass CK, Binder CJ, Uhrin P, Binder BR.** 2012. The Interferon Stimulated Gene 12 Inactivates Vasculoprotective Functions of NR4A Nuclear Receptors. Circulation Research **110:**e50-e63.
25. **Schoggins JW, Rice CM.** 2011. Interferon-stimulated genes and their antiviral effector functions. Current opinion in virology **1:**519-525.
26. **Schoggins JW, MacDuff DA, Imanaka N, Gainey MD, Shrestha B, Eitson JL, Mar KB, Richardson RB, Ratushny AV, Litvak V, Dabelic R, Manicassamy B, Aitchison JD, Aderem A, Elliott RM, Garcia-Sastre A, Racaniello V, Snijder EJ, Yokoyama WM, Diamond MS, Virgin HW, Rice CM.** 2014. Pan-viral specificity of IFN-induced genes reveals new roles for cGAS in innate immunity. Nature **505:**691-695.
27. **Li J, Ding SC, Cho H, Chung BC, Gale M, Chanda SK, Diamond MS.** 2013. A Short Hairpin RNA Screen of Interferon-Stimulated Genes Identifies a Novel Negative Regulator of the Cellular Antiviral Response. mBio **4**.
28. **Itsui Y, Sakamoto N, Kakinuma S, Nakagawa M, Sekine-Osajima Y, Tasaka-Fujita M, Nishimura-Sakurai Y, Suda G, Karakama Y, Mishima K, Yamamoto M, Watanabe T, Ueyama M, Funaoka Y, Azuma S, Watanabe M.** 2009. Antiviral effects of the interferon-induced protein guanylate binding protein 1 and its interaction with the hepatitis C virus NS5B protein. Hepatology **50:**1727-1737.
29. **Labrada L, Liang X, Zheng W, Johnston C, Levine B.** 2002. Age-dependent resistance to lethal alphavirus encephalitis in mice: analysis of gene expression in the central nervous system and identification of a novel interferon-inducible protective gene, mouse ISG12. J Virol **76:**11688 - 11703.
30. **Mody M, Cao Y, Cui Z, Tay K-Y, Shyong A, Shimizu E, Pham K, Schultz P, Welsh D, Tsien JZ.** 2001. Genome-wide gene expression profiles of the developing mouse hippocampus. Proceedings of the National Academy of Sciences **98:**8862-8867.
31. **Liu N, Zuo C, Wang X, Chen T, Yang D, Wang J, Zhu H.** 2014. miR-942 decreases TRAIL-induced apoptosis through ISG12a downregulation and is regulated by AKT. Oncotarget **5:**4959-4971.
32. **Yang D, Meng X, Xue B, Liu N, Wang X, Zhu H.** 2014. MiR-942 Mediates Hepatitis C Virus-Induced Apoptosis via Regulation of ISG12a. PLoS ONE **9:**e94501.
33. **Tantawy MA, Hatesuer B, Wilk E, Dengler L, Kasnitz N, Weiß S, Schughart K.** 2014. The Interferon-Induced Gene *Ifi27l2a* is Active in Lung Macrophages and Lymphocytes

After Influenza A Infection but Deletion of *Ifi27l2a* in Mice Does Not Increase Susceptibility to Infection. PLoS ONE **9:**e106392.

34. **Liu N, Long Y, Liu B, Yang D, Li C, Chen T, Wang X, Liu C, Zhu H.** 2014. ISG12a mediates cell response to Newcastle disease viral infection. Virology **462–463:**283-294.
35. **Uhrin P, Perkmann T, Binder B, Schabbauer G.** 2013. ISG12 is a critical modulator of innate immune responses in murine models of sepsis. Immunobiology **218:**1207-1216.
36. **Shrestha B, Diamond MS.** 2004. Role of CD8+ T Cells in Control of West Nile Virus Infection. Journal of Virology **78:**8312-8321.
37. **Keller BC, Fredericksen BL, Samuel MA, Mock RE, Mason PW, Diamond MS, Gale M.** 2006. Resistance to Alpha/Beta Interferon Is a Determinant of West Nile Virus Replication Fitness and Virulence. Journal of Virology **80:**9424-9434.
38. **Diamond MS, Shrestha B, Marri A, Mahan D, Engle M.** 2003. B Cells and Antibody Play Critical Roles in the Immediate Defense of Disseminated Infection by West Nile Encephalitis Virus. Journal of Virology **77:**2578-2586.
39. **Brien JD, Lazear HM, Diamond MS.** 2013. Propagation, Quantification, Detection, and Storage of West Nile Virus, Current Protocols in Microbiology doi:10.1002/9780471729259.mc15d03s31. John Wiley & Sons, Inc.
40. **Lanciotti RS, Kerst AJ, Nasci RS, Godsey MS, Mitchell CJ, Savage HM, Komar N, Panella NA, Allen BC, Volpe KE, Davis BS, Roehrig JT.** 2000. Rapid Detection of West Nile Virus from Human Clinical Specimens, Field-Collected Mosquitoes, and Avian Samples by a TaqMan Reverse Transcriptase-PCR Assay. Journal of Clinical Microbiology **38:**4066-4071.
41. **Daffis S, Samuel MA, Keller BC, Gale M, Jr., Diamond MS.** 2007. Cell-Specific IRF-3 Responses Protect against West Nile Virus Infection by Interferon-Dependent and -Independent Mechanisms. PLoS Pathog **3:**e106.
42. **Klein RS, Lin E, Zhang B, Luster AD, Tollett J, Samuel MA, Engle M, Diamond MS.** 2005. Neuronal CXCL10 Directs CD8+ T-Cell Recruitment and Control of West Nile Virus Encephalitis. Journal of Virology **79:**11457-11466.
43. **Fuchs A, Pinto AK, Schwaeble WJ, Diamond MS.** 2011. The lectin pathway of complement activation contributes to protection from West Nile virus infection. Virology **412:**101-109.
44. **Tacke F, Ginhoux F, Jakubzick C, van Rooijen N, Merad M, Randolph GJ.** 2006. Immature monocytes acquire antigens from other cells in the bone marrow and present them to T cells after maturing in the periphery. J Exp Med **203:**583-597.
45. **Geissmann F, Manz MG, Jung S, Sieweke MH, Merad M, Ley K.** 2010. Development of monocytes, macrophages, and dendritic cells. Science **327:**656-661.
46. **Geissmann F, Auffray C, Palframan R, Wirrig C, Ciocca A, Campisi L, Narni-Mancinelli E, Lauvau G.** 2008. Blood monocytes: distinct subsets, how they relate to dendritic cells, and their possible roles in the regulation of T-cell responses. Immunol Cell Biol **86:**398-408.
47. **Auffray C, Fogg DK, Narni-Mancinelli E, Senechal B, Trouillet C, Saederup N, Leemput J, Bigot K, Campisi L, Abitbol M, Molina T, Charo I, Hume DA, Cumano A, Lauvau G, Geissmann F.** 2009. CX3CR1+ CD115+ CD135+ common macrophage/DC precursors and the role of CX3CR1 in their response to inflammation. J Exp Med **206:**595-606.
48. **Shrestha B, Pinto AK, Green S, Bosch I, Diamond MS.** 2012. CD8+ T Cells Use TRAIL To Restrict West Nile Virus Pathogenesis by Controlling Infection in Neurons. Journal of Virology **86:**8937-8948.
49. **Richner JM, Gmyrek GB, Govero J, Tu Y, van der Windt GJW, Metcalf TU, Haddad EK, Textor J, Miller MJ, Diamond MS.** 2015. Age-Dependent Cell Trafficking Defects in

Draining Lymph Nodes Impair Adaptive Immunity and Control of West Nile Virus Infection. PLoS Pathog **11:**e1005027.

50. **Mehlhop E, Diamond MS.** 2006. Protective immune responses against West Nile virus are primed by distinct complement activation pathways. The Journal of Experimental Medicine **203:**1371-1381.
51. **Lazear HM, Lancaster A, Wilkins C, Suthar MS, Huang A, Vick SC, Clepper L, Thackray L, Brassil MM, Virgin HW, Nikolich-Zugich J, Moses AV, Gale M, Jr., Früh K, Diamond MS.** 2013. IRF-3, IRF-5, and IRF-7 Coordinately Regulate the Type I IFN Response in Myeloid Dendritic Cells Downstream of MAVS Signaling. PLoS Pathog **9:**e1003118.
52. **Lazear HM, Daniels BP, Pinto AK, Huang AC, Vick SC, Doyle SE, Gale M, Klein RS, Diamond MS.** 2015. Interferon-λ restricts West Nile virus neuroinvasion by tightening the blood-brain barrier. Science Translational Medicine **7:**284ra259-284ra259.
53. **Shrestha B, Samuel MA, Diamond MS.** 2006. CD8+ T cells require perforin to clear West Nile virus from infected neurons. J Virol **80:**119-129.
54. **Suthar MS, Diamond MS, Gale M, Jr.** 2013. West Nile virus infection and immunity. Nat Rev Microbiol **11:**115-128.
55. **Szretter KJ, Brien JD, Thackray LB, Virgin HW, Cresswell P, Diamond MS.** 2011. The Interferon-Inducible Gene viperin Restricts West Nile Virus Pathogenesis. Journal of Virology **85:**11557-11566.
56. **Suthar MS, Ma DY, Thomas S, Lund JM, Zhang N, Daffis S, Rudensky AY, Bevan MJ, Clark EA, Kaja M-K, Diamond MS, Gale M, Jr.** 2010. IPS-1 Is Essential for the Control of West Nile Virus Infection and Immunity. PLoS Pathog **6:**e1000757.
57. **Daffis S, Suthar MS, Szretter KJ, Gale M, Jr., Diamond MS.** 2009. Induction of IFN-β and the Innate Antiviral Response in Myeloid Cells Occurs through an IPS-1-Dependent Signal That Does Not Require IRF-3 and IRF-7. PLoS Pathog **5:**e1000607.
58. **Samuel MA, Diamond MS.** 2005. Alpha/Beta Interferon Protects against Lethal West Nile Virus Infection by Restricting Cellular Tropism and Enhancing Neuronal Survival. Journal of Virology **79:**13350-13361.
59. **Lazear HM, Pinto AK, Vogt MR, Gale M, Diamond MS.** 2011. Beta Interferon Controls West Nile Virus Infection and Pathogenesis in Mice. Journal of Virology **85:**7186-7194.
60. **Suthar MS, Brassil MM, Blahnik G, Gale M.** 2012. Infectious Clones of Novel Lineage 1 and Lineage 2 West Nile Virus Strains WNV-TX02 and WNV-Madagascar. Journal of Virology **86:**7704-7709.
61. **Shrestha B, Gottlieb DI, Diamond MS.** 2003. Infection and injury of neurons by West Nile Encephalitis virus. J Virol **77:**13203-13213.
62. **Samuel MA, Morrey JD, Diamond MS.** 2007. Caspase-3 dependent cell death of neurons contributes to the pathogenesis of West Nile virus encephalitis. J Virol **81:**2614-2623.
63. **Labrada L, Liang XH, Zheng W, Johnston C, Levine B.** 2002. Age-Dependent Resistance to Lethal Alphavirus Encephalitis in Mice: Analysis of Gene Expression in the Central Nervous System and Identification of a Novel Interferon-Inducible Protective Gene, Mouse ISG12. Journal of Virology **76:**11688-11703.
64. **Wie S-H, Du P, Luong TQ, Rought SE, Beliakova-Bethell N, Lozach J, Corbeil J, Kornbluth RS, Richman DD, Woelk CH.** 2013. HIV Downregulates Interferon-Stimulated Genes in Primary Macrophages. Journal of Interferon & Cytokine Research **33:**90-95.
65. **Pommerenke C, Wilk E, Srivastava B, Schulze A, Novoselova N, Geffers R, Schughart K.** 2012. Global Transcriptome Analysis in Influenza-Infected Mouse Lungs Reveals the Kinetics of Innate and Adaptive Host Immune Responses. PLoS ONE **7:**e41169.

66. **Clarke P, Leser JS, Bowen RA, Tyler KL.** 2014. Virus-Induced Transcriptional Changes in the Brain Include the Differential Expression of Genes Associated with Interferon, Apoptosis, Interleukin 17 Receptor A, and Glutamate Signaling as Well as Flavivirus-Specific Upregulation of tRNA Synthetases. mBio **5**.

67. **Itsui Y, Sakamoto N, Kakinuma S, Nakagawa M, Sekine-Osajima Y, Tasaka-Fujita M, Nishimura-Sakurai Y, Suda G, Karakama Y, Mishima K, Yamamoto M, Watanabe T, Ueyama M, Funaoka Y, Azuma S, Watanabe M.** 2009. Antiviral effects of the interferon-induced protein guanylate binding protein 1 and its interaction with the hepatitis C virus NS5B protein. Hepatology **50:**1727-1737.

68. **Qi Y, Li Y, Zhang Y, Zhang L, Wang Z, Zhang X, Gui L, Huang J.** 2015. IFI6 Inhibits Apoptosis via Mitochondrial-Dependent Pathway in Dengue Virus 2 Infected Vascular Endothelial Cells. PLoS ONE **10:**e0132743.

69. **Makovitzki-Avraham E, Daniel-Carmi V, Alteber Z, Farago M, Tzehoval E, Eisenbach L.** 2013. The human ISG12a gene is a novel caspase dependent and p53 independent pro-apoptotic gene, that is overexpressed in breast cancer. Cell Biology International Reports **20:**37-46.

70. **Li S, Xie Y, Zhang W, Gao J, Wang M, Zheng G, Yin X, Xia H, Tao X.** 2014. Interferon alpha-inducible protein 27 promotes epithelial–mesenchymal transition and induces ovarian tumorigenicity and stemness. Journal of Surgical Research **193:**255-264.

71. **Hsieh WL, Huang YH, Wang TM, Ming YC, Tsai CN, Pang JHS.** 2015. IFI27, a novel epidermal growth factor-stabilized protein, is functionally involved in proliferation and cell cycling of human epidermal keratinocytes. Cell Proliferation **48:**187-197.

72. **Schoggins JW, Wilson SJ, Panis M, Murphy MY, Jones CT, Bieniasz P, Rice CM.** 2011. A diverse range of gene products are effectors of the type I interferon antiviral response. Nature **472:**481-485.

73. **Fensterl V, Wetzel JL, Ramachandran S, Ogino T, Stohlman SA, Bergmann CC, Diamond MS, Virgin HW, Sen GC.** 2012. Interferon-Induced Ifit2/ISG54 Protects Mice from Lethal VSV Neuropathogenesis. PLoS Pathog **8:**e1002712.

74. **Garcia MR, Ledgerwood L, Yang Y, Xu J, Lal G, Burrell B, Ma G, Hashimoto D, Li Y, Boros P, Grisotto M, van Rooijen N, Matesanz R, Tacke F, Ginhoux F, Ding Y, Chen SH, Randolph G, Merad M, Bromberg JS, Ochando JC.** 2010. Monocytic suppressive cells mediate cardiovascular transplantation tolerance in mice. J Clin Invest **120:**2486-2496.

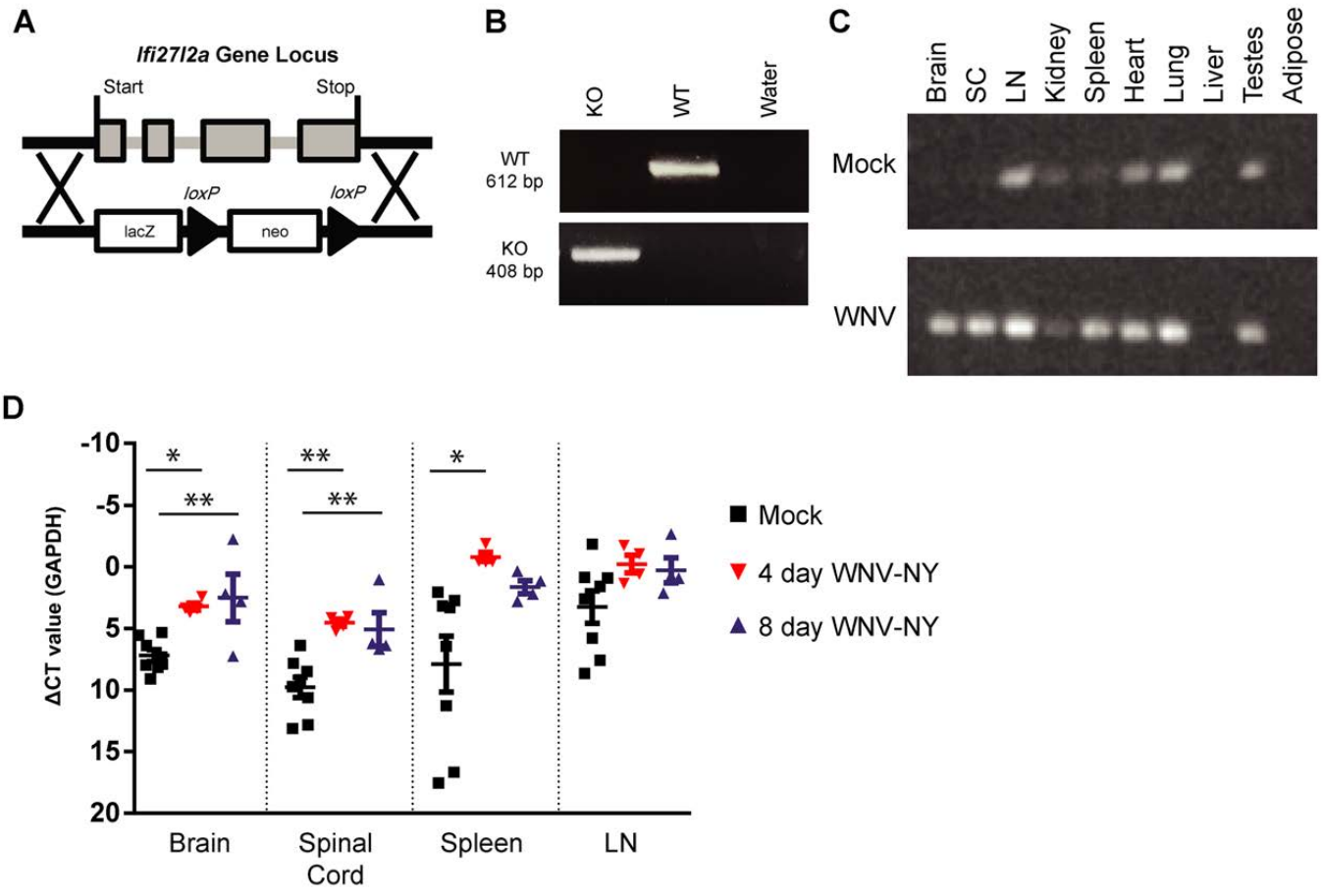

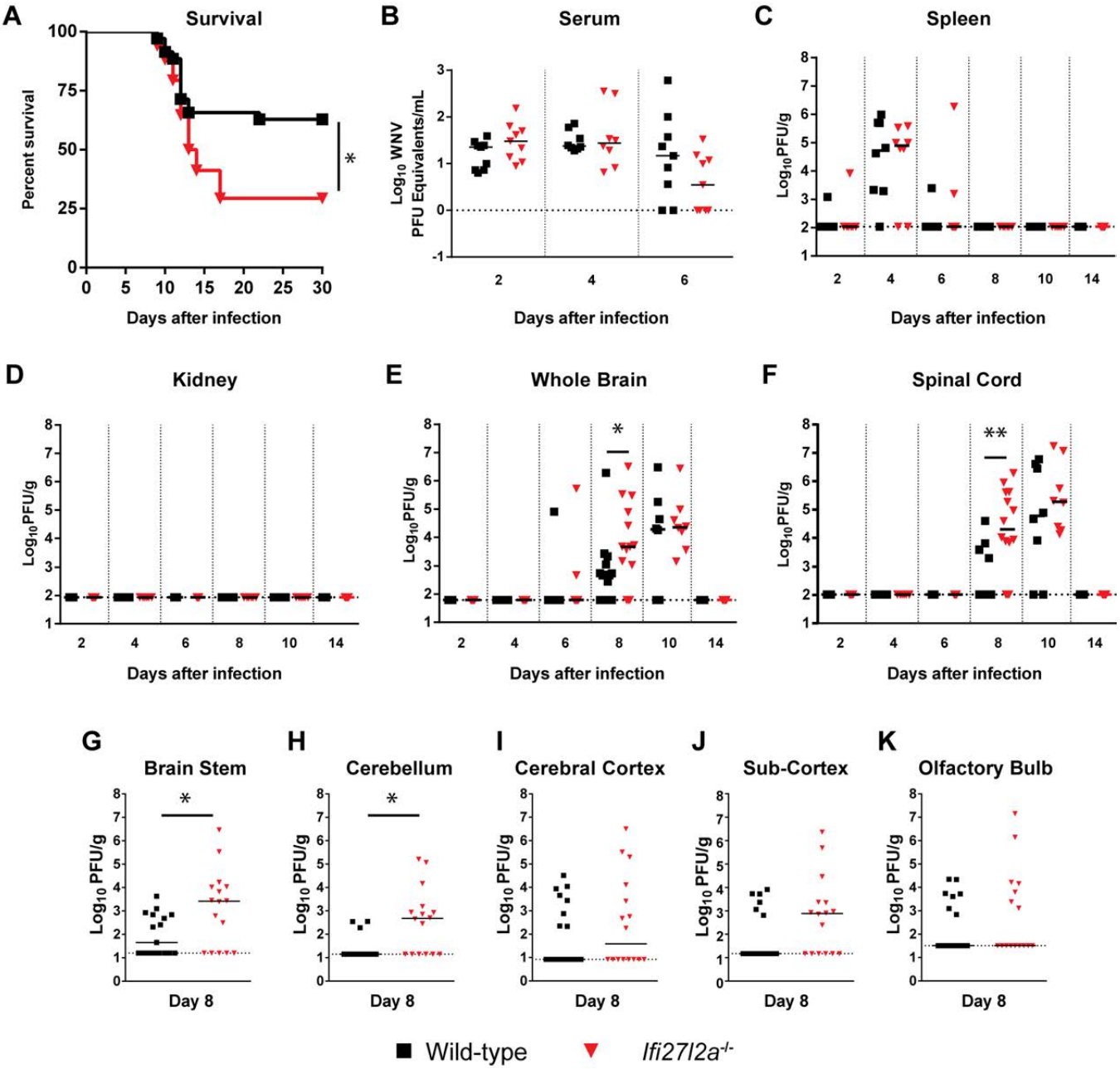

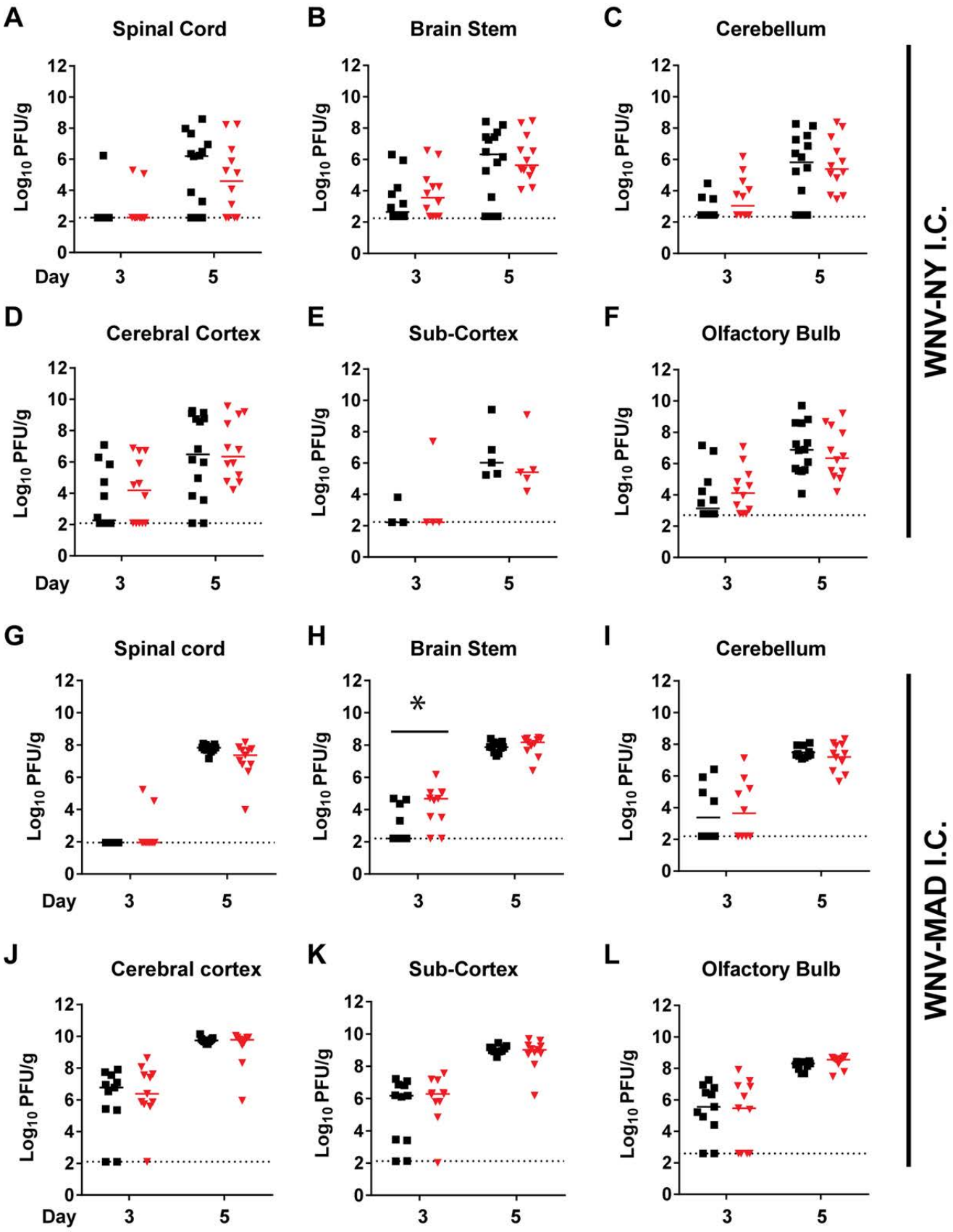

JVI Journal of Virology

Journal of Virology